Expansion of a bacterial operon during cancer treatment ameliorates drug toxicity

Authors: Kai R. Trepka[1]†, Wesley A. Kidder[2,3]†, Than S. Kyaw[1], Christine A. Olson[1], Vaibhav Upadhyay[1], Cecilia Noecker[1], Dalila Stanfield[3], Paige Steiding[3], Peter Spanogiannopoulos[1], Darren Dumlao[4], Jessie A. Turnbaugh[1], Matthew D. Stachler[5], Erin L. Van Blarigan[3,6,7], Alan P. Venook[2,3], Chloe E. Atreya[2,3], Peter J. Turnbaugh[1,8]*

Affiliations:

[1]Department of Microbiology and Immunology, University of California San Francisco; San Francisco, USA

[2]Department of Medicine, Division of Hematology and Oncology, University of California San Francisco; San Francisco, USA

[3]UCSF Helen Diller Family Comprehensive Cancer Center; San Francisco, USA

[4]Department of Gastroenterology, University of California San Francisco; San Francisco, USA

[5]Department of Pathology, University of California San Francisco; San Francisco, USA

[6]Department of Epidemiology and Biostatistics, University of California San Francisco; San Francisco, USA

[7]Department of Urology, University of California San Francisco; San Francisco, USA

[8]Chan Zuckerberg Biohub-San Francisco; San Francisco, USA

*Corresponding author. Email: Peter.Turnbaugh@ucsf.edu

† These authors contributed equally to this work

One Sentence Summary: Gut microbial enzymes can be used to predict and prevent anticancer drug toxicity.

Abstract: Dose-limiting toxicities remain a major barrier to drug development and therapy, revealing the limited predictive power of human genetics. Herein, we demonstrate the utility of a more comprehensive approach to studying drug toxicity through longitudinal study of the human gut microbiome during colorectal cancer (CRC) treatment (NCT04054908) coupled to cell culture and mouse experiments. 16S rRNA gene and metagenomic sequencing revealed significant shifts in gut microbial community structure during treatment with oral fluoropyrimidines, which was validated in an independent cohort. Gene abundance was also markedly changed by oral fluoropyrimidines, including an enrichment for the *preTA* operon, which is sufficient for the inactivation of active metabolite 5-fluorouracil (5-FU). Higher levels of *preTA* led to increased 5-FU depletion by the gut microbiota grown *ex vivo*. Germ-free and antibiotic-treated mice had increased fluoropyrimidine toxicity, which was rescued by colonization with the mouse gut microbiota, *preTA+ E. coli*, or CRC patient stool with high *preTA* levels. *preTA* abundance was negatively associated with patient toxicities. Together, these data support a causal, clinically relevant interaction between a human gut bacterial operon and the dose-limiting side effects of cancer treatment. Our approach is generalizable to other drugs, including cancer immunotherapies, and provides valuable insights into host-microbiome interactions in the context of disease.

INTRODUCTION

Dose-limiting toxicities pose a major challenge in drug development *(1)*. Decades of pharmacogenomic research have identified host alleles responsible for variable drug metabolism, yet clinical implementation has lagged due to persistent unexplained variability in toxicity *(2, 3)*. The gut microbiome complements and extends host pathways of drug metabolism, with depletion of hundreds of pharmaceuticals following *in vitro* incubation with gut strains *(4, 5)*. However, the impact of microbial drug metabolism on toxicity *in vivo* remains underexplored.

Despite advances in immunotherapy, cytotoxic chemotherapies such as fluoropyrimidines remain a cornerstone of gastrointestinal cancer treatment *(6)*. A significant obstacle in fluoropyrimidine therapy is high interpatient variability in toxicity, necessitating dose adjustments in 35% of patients and therapy discontinuation in 10% *(7)*. The widely-used oral fluoropyrimidine capecitabine (CAP) is a prodrug that is converted to 5-fluorouracil (5-FU), which kills cells through disruption of DNA synthesis and RNA processing *(8)*. Toxic 5-FU is cleared to inactive dihydrofluorouracil (DHFU) by homologous host and microbial enzymes (DPYD and PreTA, respectively) *(9, 10)*. While rare patient DPYD sequence variants are associated with severe CAP toxicity *(11)*, host genetic variation and other risk factors cannot explain extensive inter-subject variation in pharmacokinetics and toxicity *(12–14)*. The gut microbiome varies widely between colorectal cancer (CRC) patients *(15)*, offering a potential source of variability in toxicity. However, the impact of microbial *preTA* on predicting and preventing CAP toxicity remains unknown.

Here, we explore the role of microbial *preTA* in toxicity through the combined use of longitudinal studies of CRC patients receiving chemotherapy and follow-on studies *ex vivo* and *in vivo*. Together, our results highlight the importance of considering drug-microbe interactions to gain a more comprehensive view of mechanisms of variability in drug toxicity.

RESULTS

Oral fluoropyrimidines perturb gut microbial community structure

We conducted the Gut microbiome and Oral fluoropyrimidine (GO) clinical study (ClinicalTrials.gov ID NCT04054908), a prospective longitudinal study investigating the impact of oral fluoropyrimidines on the gut microbiome. Stool was collected at 7 timepoints spanning pre-treatment to post-cycle 3 of chemotherapy **(Fig. 1A)**. Of the 52 patients enrolled, 40 submitted at least one stool sample **(Figs. S1)**. Patients were distributed among three sub-cohorts (**Table S1**): (A) CAP as monotherapy or part of a standard-of-care regimen (n = 21); (B) TAS-102 (trifluridine/tipiracil, n = 9); (C), CAP with bevacizumab and pembrolizumab immunotherapy (patients participating on ClinicalTrials.gov ID NCT03396926, n = 10). The 40 participants had a mean age of 52.5±10.5 y; 50% were male, 78% identified as white, and 7.5% identified as Hispanic or Latino ethnicity (**Table S1**). 83% of patients were TNM stage III-IV and 68% had prior surgery (**Table S1**).

We utilized 16S rRNA gene sequencing to assess longitudinal shifts in the gut microbiota during cancer therapy. To better power our analysis, we sought to capture the overall longitudinal trends across all patients in all sub-cohorts. The combined dataset represented 217 samples from 40 patients with 67,915±3,744 high-quality reads per sample (**Data File S1**). Treatment was significantly associated with microbiota composition (**Fig. S2A**). For linear modeling, we

truncated the data at 50 days post-Cycle 1 treatment initiation to avoid the influence of long-duration outliers and patient drop-out on model results (**Fig. S1B**). Alpha diversity and amplicon sequence variants (ASVs) were analyzed using a mixed-effects model, with time as a fixed effect and Patient ID as a random effect (see *Methods*). We observed a significant decrease in Shannon diversity index on treatment (**Fig. 1B**). Alternative markers of diversity trended lower but did not reach statistical significance (**Figs. S2B,C**). We identified 43 differentially abundant ASVs, including 16 that increased and 27 that decreased over time (**Fig. 1C, Fig. S2F, Data File S2**). The shift in ASV abundance during Cycle 1 and Trough relative to baseline were correlated **(Fig. S2D)**, with similar ASV shifts observed in each sub-cohort individually **(Fig. S2E)**. Treatment-associated ASVs were from 11 bacterial orders (**Fig. 1D**). The depleted ASVs included a cluster of *Oscillospirales,* whereas the enriched ASVs were more phylogenetically dispersed (**Fig. 1E**). Remarkably, our list of treatment-associated ASVs was significantly associated with sensitivity to CAP and 5-FU in mono-culture (**Fig. 1F**), suggesting that at least some observed changes were due to the direct impact of fluoropyrimidines on the gut microbiota.

We sought to replicate these observations using an independent patient cohort. We obtained previously published *(16)* 16S rRNA gene sequencing data from 33 CRC patients treated with CAP in the Netherlands (NE dataset, **Fig. S3A).** We observed a decline in ASV number, Inverse Simpson index, and Shannon index on treatment (**Fig. S3B-D).** Possibly due to the lower sample size and/or later sampling time relative to fluoropyrimidine treatment, we only detected a single significantly decreased ASV, mapped to the *Anaerovoracaceae* (**Fig. S3E,F**). Consistent with the GO dataset, the shift in ASV abundance in Cycle 3 was similar at Trough relative to Baseline (**Fig. S3G**). Despite many methodological explanations for a cohort effect, ASV-level shifts with respect to treatment were significantly associated between the GO and NE studies (**Fig. S3H**). Thus, it is possible to identify consistent shifts in the gut microbiota in CRC patients treated with oral fluoropyrimidines.

Chemotherapy selects for gut microbial pyrimidine metabolism genes

Given the numerous potential mechanisms through which the gut microbiome can influence cancer progression and drug response, we sought to use metagenomic sequencing to develop a mechanistic hypothesis as to the consequences of fluoropyrimidine-induced shifts in the gut microbiome for drug response. Our metagenomic GO dataset represents 229 stool samples from 40 patients, with 26.02±10.87 million high quality reads per sample (7.68±0.22 Gbp, **Data File S3**). The distance to baseline based on metagenomic KEGG Orthologous group (KO) abundances (central log ratio (CLR)-Euclidean ordination) spiked during Cycle 1 with subsequent partial recovery (**Fig. S4A**); therefore, we opted to focus on KO abundances in Cycle 1 versus Baseline. Consistent shifts in KO abundance were detectable by principal coordinate analysis (**Fig. 2A**), reflecting 152 KOs with significantly altered relative abundance (**Fig. 2B, Data File S4**). Notably, nearly all (149) of these KOs increased in abundance, with the exception of 3 KOs that decreased: K06989 (aspartate dehydrogenase), K20626 (lactoyl-CoA dehydratase subunit alpha), and K20461 (lantibiotic transport system permease protein). Gene set enrichment analysis of the 149 enriched genes highlighted multiple pathways relevant to fluoropyrimidine metabolism, including pyrimidine metabolism, pantothenate and CoA biosynthesis, and β-alanine metabolism (**Fig. 2C**).

Inspection of the KOs within these pathways (**Fig. 2D, Fig. S4B**) revealed a significant increase in the abundance of uracil phosphoribosyltransferase (*upp,* K00757), which is a well-established contributor to bacterial drug sensitivity *(9, 17, 18)*. Consistent with this trend, levels of pyrimidine-nucleoside phosphorylase (*pdp,* K00756) increased following the initiation of treatment. In turn, multiple genes in the bacterial pathway for 5-FU inactivation were enriched, including the bacterial dihydropyrimidine dehydrogenase (*preT,* K17722 and *preA*, K17723) responsible for the reduction of 5-FU to DHFU and dihydropyrimidinase (*hydA,* K01464) that further processes DHFU to α-Fluoro-β-ureidopropionic acid (FUPA). We further validated enrichment of pyrimidine-metabolizing pathways and genes using UniRef90 and enzyme class (EC) annotation schemes (**Figs. S4C-F**).

Given the clear clinical implications of the inactivation of 5-FU to DHFU *(11, 12)* and our prior work on the *preTA* operon *(9)*, we further analyzed the bacterial taxa that explain the observed treatment-associated enrichment in *preTA* levels. Analysis of stratified gene abundance data revealed that *Anaerostipes hadrus*, *Escherichia* spp., *Eubacterium siraeum*, and *Citrobacter* spp. accounted for >99% of *preTA* **(Fig. 2E)**. Consistent with the observed inter-individual heterogeneity in the dominant *preTA+* species, no single ASV from these species was significantly enriched during Cycle 1 (false discovery rate > 0.2, mixed-effects model with Treatment Group as a fixed effect and Patient as a random effect). In contrast, the aggregated abundance of all *preTA+* ASVs significantly increased following fluoropyrimidine treatment in both the GO (**Fig. 2F**) and NE (**Fig. S3I**) cohorts. Our aggregate metric for *preTA+* ASV abundance by 16S rRNA gene sequencing was significantly associated with *preTA* gene abundance by metagenomics (**Fig. 2G**).

We further validated these findings by testing the functional relevance of shifts in the abundance of *preTA* for 5-FU metabolism. Baseline stool samples from 3 patients with variable baseline *preTA* were cultured *ex vivo* in the presence of vehicle, 5-FU, or CAP for 48 hours. Both 5-FU and its oral prodrug CAP significantly inhibited overall bacterial growth (**Fig. S5A**), consistent with prior evidence for CAP bioactivation by human gut bacteria *(5, 9)*. 16S rRNA gene sequencing of the endpoint microbiotas revealed decreased diversity in response to CAP and 5-FU (**Fig. S5B**) and significantly altered community structure (**Fig. S5C**). The shifts in ASV abundance in response to CAP and 5-FU were significantly associated (**Fig. S5D**). Quantification of 5-FU levels at the endpoint by LC-MS/MS revealed marked differences between each *ex vivo* community that were significantly associated with *preTA* abundance (**Fig. 2H**). The source of *preTA* was primarily *E. coli* (**Fig. 2I**).

Microbiota depletion exacerbates CAP toxicity

These data raised the intriguing hypothesis that an expansion of *preTA+* bacteria following the initiation of fluoropyrimidine treatment could potentially mitigate gastrointestinal (GI) side effects. However, there was no established mouse model of oral fluoropyrimidine toxicity, necessitating extensive experimentation to establish such a model (*data not shown*). We ultimately selected a daily dose of 1,500 mg/kg CAP, which is equivalent to a daily human dose of 4500 mg/m^2 *(19)* and slightly higher than total daily GO study dose (1700-2500 mg/m^2).

CAP was administered by oral gavage to 8-week old female C57BL/6J mice (n = 8-12 mice/group; **Fig. 3A, Table S2**). CAP led to significant weight loss relative to vehicle controls (**Figs. 3B,C**) without any significant differences in body composition (**Figs. S6A-C**), small

intestine length (**Fig. S6D**), or spleen weight (**Fig. S6E**). We detected clear evidence of colonic inflammation, including decreased colon length (**Fig. 3D**) and increased stool levels of lipocalin-2 (**Fig. 3E**). Hind paw thermal hyperalgesia was significantly worsened (**Fig. 3F**), indicating that this mouse model mimics aspects of the CAP-induced hand-foot syndrome *(20)*, a common reason for CAP dose modifications *(7)*. The severity of these phenotypes were significantly associated (**Fig. 3G**), motivating the use of weight loss as a proxy in subsequent experiments.

CAP significantly altered the gut microbiota in our mouse model. We observed a significant decrease in Shannon diversity index (**Fig. S7A**). CAP treatment was significantly associated with microbiota composition (**Fig. S7B**). We identified 64 differentially abundant genera in CAP-treated but not vehicle-treated mice, including 37 that increased and 27 that decreased over time (**Fig. S7C, Data File S5**). Treatment associated-genera were from multiple bacterial orders, including many Clostridiales members **(Fig. S7D**).

Having established our mouse model, we tested if the overall gut microbiota impacts CAP toxicity. To deplete the gut microbiota, 6-8 week old female C57BL/6J mice were treated with a cocktail of broad-spectrum antibiotics (ampicillin, vancomycin, neomycin, and metronidazole; AVNM) or vehicle for one week prior to CAP administration (**Fig. 4A, Table S2**). As expected, AVNM significantly decreased total colonization level and increased cecal weight (**Fig. S8**). Weight loss was significantly accelerated in AVNM-treated mice (**Fig. 4B,C**), resulting in significantly decreased survival relative to vehicle controls (**Fig. 4D**).

These effects were validated in gnotobiotic mice. We compared CAP toxicity in germ-free (GF), conventionalized (ex-GF, CONV-D), and conventionally-raised (CONV-R) 6-8 week old female C57BL/6J mice (**Fig. 4E, Table S2**). Because GF mice experience higher serum 5-FU levels following CAP administration *(9),* we reduced the dose of CAP to 1,100 mg/kg by daily oral gavage. Consistent with our antibiotic depletion data, CAP led to significantly enhanced weight loss (**Fig. 4F,G**) and decreased survival (**Fig. 4H**) in GF mice relative to CONV-R or CONV-D mice. Taken together, these results indicate that an intact microbiota at the time of CAP treatment is critical to avoid increased drug toxicity.

Microbial *preTA* rescues oral fluoropyrimidine toxicity

We leveraged this toxicity model to test the impact of bacterial *preTA* on CAP toxicity alone and in the context of a complex human gut microbiota. First, 6-8 week old female C57BL/6J CONV-R mice were provided 1 g/L streptomycin in drinking water to enable the stable engraftment of isogenic Δ*preTA* or *preTA* overexpressing (*preTA*$^{++}$) *E. coli* MG1655 as described previously *(9)* (**Fig. 5A, Table S2**). *E. coli* colonization levels were similar between groups (**Fig. 5B**). Remarkably, the *preTA*$^{++}$ strain was sufficient to rescue CAP-induced weight loss (**Fig. 5C,D**) and survival relative to the Δ*preTA* strain (**Fig. 5E**). These results were validated in mono-colonized mice (**Fig. S9**). Next, we colonized GF 6-8 week old male C57BL/6J mice with baseline stool samples collected from CRC patients in the GO study with varying *preTA* abundance (**Fig. 5F, Table S2**). We quantified *preTA* levels at baseline via metagenomic sequencing, finding measurable baseline *preTA* in 18/31 mice with evaluable stool (**Fig. 5G**). Consistent with our results with *E. coli*, mice with measurable baseline *preTA* experienced lower weight loss (**Fig. 5H,I**) and increased colon length (**Fig. 5J**).

Finally, we sought to assess the translational relevance of our findings in this mouse model of toxicity. We performed a retrospective chart review of oral fluoropyrimidine-associated side effects reported on the GO study. The majority (21/40) of GO subjects had at least one documented toxicity-related event, including 6 subjects with documented CAP dose reductions during the study (**Fig. 6A**). Consistent with our results in mice, *preTA* was significantly more abundant in patients without reported evidence of clinically significant toxicity (**Fig. 6B**). Using *preTA* level to predict host toxicity with univariate receiver operating characteristic (ROC) curve analysis, we achieved an area under the curve (AUC) = 0.68 in patients and AUC = 0.85 in humanized mice (**Fig. S10A-B**). In addition to links to host drug toxicity, we noted a correlation between the magnitude of microbiota disruption and *preTA* abundance. Patients with high *preTA* maintained higher microbial diversity (**Fig. 6C**) and less deviation in microbial community structure relative to baseline (**Fig. 6D**).

DISCUSSION

This study underscores the complex and clinically meaningful interplay between the gut microbiome and oral fluoropyrimidines, a commonly-used chemotherapy. Longitudinal analyses of patient stool showed that chemotherapy has broad impacts on human gut microbial community structure, gene, and pathway abundance. This includes an enrichment for the bacterial *preTA* operon, which enables the inactivation of 5-FU to DHFU. We established and implemented a mouse model of CAP toxicity, allowing us to demonstrate that CAP toxicity is microbiome-dependent and that high levels of *preTA* expression are sufficient to control CAP toxicity. Together, these findings provide a *proof-of-concept* for the "reverse translation" of observations from cancer patients to gain mechanistic insight from follow-on mouse and cell culture experiments.

Remarkably, we were able to detect consistent oral fluoropyrimidine-associated shifts in the gut microbiota in distinct patient cohorts from the United States and the Netherlands. This is particularly surprising given the geographical differences in the human gut microbiota *(21)* and prior literature emphasizing the difficulties in finding consistent differences across cohorts for cancer immunotherapy *(22)*. The longitudinal nature of frequent sampling is a strength of our approach, allowing us to assess changes in the microbiome over time by controlling for within-subject differences that confound cross-sectional studies. These results suggest that oral chemotherapy has a more robust and reproducible impact on the human gut microbiota due to its ability to directly alter bacterial growth, as opposed to more indirect mechanisms at play for immunotherapy.

While we opted to focus on *preTA*, our results highlight numerous mechanisms through which chemotherapy-induced microbiome shifts could influence treatment outcomes. For example, we noted an overall decrease in microbial diversity following treatment, which has been associated with fluoropyrimidine-induced diarrhea in prior studies *(23)*. Multiple bacterial taxa associated with immunotherapy response were depleted following chemotherapy, including the positively associated *Faecalibacterium prausnitzii* and negatively associated *Oscillospiraceae* species *(24, 25)*. Notably, the most significantly enriched gene family was multidrug/hemolysin ABC transporter component *cylA* (K11050), a known virulence factor *(26)* that has also been implicated in inflammatory bowel disease *(27)*. Thus, shifts in the microbiome following oral fluoropyrimidine treatment likely results in a complex combination of beneficial, neutral, and deleterious shifts in gut microbial ecology and host-microbiome interactions.

Our results emphasize the complex role the gut microbiome can play in chemotherapy response. In this study, we utilized a novel mouse model to demonstrate that CAP toxicity is microbiome-dependent, consistent with data in human subjects showing heightened toxicity of CAP-containing regimens in antibiotic-pretreated patients *(28)*. On the other hand, extensive prior literature has shown that antibiotics alleviate the GI toxicity of the anti-cancer drug irinotecan (SN-38) in rats and humans by preventing bacterial reactivation of inactive SN-38G *(29, 30)*. Since treatment regimens such as XELIRI and FOLFIRI combine both fluoropyrimidines and irinotecan *(31)*, use of antibiotics may worsen CAP toxicity while alleviating irinotecan toxicity, highlighting a clinical need to develop targeted microbial manipulations rather than relying on broad-spectrum antibiotics.

The observation that bacterial *preTA* is sufficient to control CAP toxicity in mice has clear translational relevance, raising the potential to utilize current or next-generation probiotics to

ameliorate GI toxicity in cancer patients. GI toxicities usually present early during CAP treatment *(32–34)*. This observation is consistent with decreased toxicity following *preTA* expansion during treatment. Notably, prior studies have shown a benefit of fecal microbiota transplantation (FMT) and probiotics containing *Lactobacillus reuteri (35, 36)*, both of which could be in part driven by increased *preTA* and thus enhanced 5-FU inactivation within the gut lumen. A critical next step is to assess the trade-offs between decreased toxicity and efficacy, especially given prior data suggesting that high levels of *preTA* can interfere with the anti-tumor effects of CAP *(9)*. More broadly, probiotic strains that express *preTA* could be a valuable tool to treat pyrimidine-related toxicity in other conditions, potentially depriving cancer cells of uracil in pancreatic ductal adenocarcinoma *(37)* and clearing excess uracil in patients with clinical DPYD deficiency *(38)*.

Low *preTA* levels were predictive of increased adverse effects in humanized mice and patients, providing a *proof-of-concept* for the use of microbial "genotyping" as a tool for predicting toxicity. Baseline *preTA* serves as a mechanistic microbial predictor of toxicity with near-perfect class separation in humanized $Dpyd^{+/+}$ mice and an AUC of 0.68 in the GO patient cohort. Meanwhile, clinical predictors in $DPYD^{+/+}$ patients combining age, body surface area, type of treatment regimen, and creatinine levels achieve an AUC of 0.68 when predicting global Grade 3+ toxicity *(39)*, and comprehensive DPYD genotyping alone has an AUC < 0.5 for predicting global Grade 2+ toxicity *(40)*. With refinement and integration with known clinical variables and host genetics, our microbiome-based prediction algorithm could help address long-standing challenges in avoiding the severe toxicities associated with fluoropyrimidine drugs.

While this work emphasizes the crucial role of drug-microbiome interactions in cancer therapy, key translational questions remain. Heterogeneous patient populations, combinatorial treatment regimens, and small sub-cohort sample sizes limited our ability to test the impact of immunotherapy, radiation, and biologics on the microbiome. Since host DPYD deficiency is associated with life-threatening side effects *(14)*, future work seeking to understand toxicity should integrate genetics of both host *DPYD* and microbial *preTA*. Data in human subjects suggests that orally delivered fluoropyrimidines have ten times less neutropenia but comparable GI toxicity to infusional 5-FU *(41, 42)*. The degree to which bacterial *preTA* is better able to mitigate toxicities following oral versus intravenous delivery is an important area for future studies.

Overall, our results highlight the complex and bidirectional relationship between the gut microbiome and oral fluoropyrimidine chemotherapy and the consequences of this relationship for host drug toxicity. Integrating longitudinal microbiome analysis with *in vivo* and *ex vivo* experiments, we show that fluoropyrimidine metabolism gene *preTA* is a critical human gut bacterial mediator of oral fluoropyrimidine toxicity. This microbial operon serves as a biomarker for predicting and a novel target for controlling dose-limiting toxicities. Our findings underscore the necessity of considering the microbiome as an integral component in the pharmacological landscape, paving the way for microbiota-based precision therapy.

MATERIALS AND METHODS

Study design

The Gut microbiome and Oral fluoropyrimidines (GO) study was an observational clinical study registered at ClinicalTrials.gov under the identifier NCT04054908. All participants provided informed consent. The study was approved by the UCSF Institutional Review Board. Participants were recruited and sampled, without any compensation, at UCSF from the study start date (2018/04/13) to end date (2022/06/30). Inclusion criteria included: (1) 18 years or older, (2) histologically confirmed colorectal adenocarcinoma, and (3) expected to receive oral fluoropyrimidine therapy. Patients who met any of the following criteria were excluded: (1) known HIV positive diagnosis, (2) chemotherapy, biologic or immunotherapy in the previous 2 weeks, (3) exposure to ≥2 weeks antibiotics in the last 6 months, (4) exposure to antibiotics in the past 4 weeks. Patients were enrolled to one of three cohorts: Cohort A received oral CAP as part of standard-of-care therapy; Cohort B received TAS-102 (trifluridine/tipiracil) ± Y-90 radioembolization *(43)*; Cohort C received CAP + immunotherapy (pembrolizumab) + bevacizumab as part of a separate clinical trial (NCT03396926). Patients with concurrent rectal radiation therapy (RT) were originally excluded, but the eligibility criteria was amended to include patients with concurrent rectal RT to increase enrollment. CAP and TAS-102 tablets were prescribed according to FDA labels for oral dosing. CAP tablets were taken twice daily on days 1–14 of a 21-day Cycle (no RT) or on days of radiation only (RT); TAS-102 tablets were taken twice daily on days 1–5 and 8–12 of a 28-day Cycle. Stool collection occurred at home before chemotherapy initiation and on day 1 of Cycles 1, 2, 3. During Cycle 1, stool was also collected at day 3 and midpoint (day 7 for Cohorts A, C; day 10 for cohort B). Actual collection days are plotted in **Fig. S1**. Stool samples were collected on fecal occult blood test (FOBT) cards for all time points. Additional bulk scoop samples were collected at baseline for culturing. Stool was stored at −80 °C upon receipt at UCSF. 229 stool samples from 40 participants on FOBT cards were ultimately evaluable; 4 samples were not evaluable due to insufficient extracted DNA quantity.

Resources Table

Reagent	**Source**	**Catalog Number**
Capecitabine	Fisher Scientific	50148375
5-fluorouracil	Millipore Sigma	F6627
5-fluorouracil-$^{13}C,^{15}N_2$	Santa Cruz Biotechnology	217189
Citric acid	Thomas Scientific	C752W30
Sodium citrate dihydrate	Fisher Scientific	18613454
Gum arabic	Spectrum Chemicals	GU113
Escherichia coli ΔpreTA	*(9)*	N/A

Escherichia coli preTA^{++}	*(9)*	N/A
Bacto Brain Heart Infusion (broth)	Fisher Scientific	237500
L-Cysteine HCl	Fisher Scientific	C81020
Hemin	Fisher Scientific	51280
Menadione (Vitamin K)	Fisher Scientific	102259
Lysogeny broth (LB)	Millipore Sigma	L3152
Eosin Methylene Blue (EMB) agar	Thomas Scientific	C5701
Streptomycin	Thomas Scientific	S6501
Neomycin	Neta Scientific	SIAL-N1876
Azithromycin	Neta Scientific	FISHUCOP-A20765G
Vancomycin	Thomas Scientific	C752X68
Metronidazole	Neta Scientific	SIAL-M1547-25G
Sucrose	Thomas Scientific	C752W82
Dimethyl sulfoxide	Millipore Sigma	D8418
Mouse Lipocalin-2/NGAL DuoSet ELISA	Fisher Scientific	DY185705
ZymoBIOMICS 96 MagBead DNA Kit	Zymo Research	D4302
SYBR Green I	Millipore Sigma	S9430
Nuclease-free water	Life Tech	0977-023
Phusion High-Fidelity PCR Kit	Thermo Scientific	F553L
QIAquick Gel Extraction Kit	Qiagen	28604
KAPA Library Quantification Kit	Roche	KK4824
MiSeq Reagent Kit v3 (600 cycles)	Illumina	MS-102-3003
Illumina DNA Prep, (M) Tagmentation (96 Samples, IPB)	Illumina	20060059

Quant-iT Picogreen dsDNA Kit	Invitrogen	P7589
SYBR Select	Life Technologies	4472908
Wildtype C57BL/6J mice	Jackson Labs	000664
Standard chow diet (SPF)	LabDiet	5058
Standard autoclaved chow diet	LabDiet	5021
BreatheEasy Covers	Millipore Sigma	Z380059

DNA extraction

ZymoBIOMICs 96 MagBead DNA Kit was used for DNA extractions from mouse and human stool. 750 µL of lysis solution was added to fecal aliquots (20-50 mg) in lysis tubes. Samples were homogenized with 5 min bead beating (Mini-Beadbeater-96, BioSpec), followed by 5 min room temperature (RT) incubation, and repeat 5 min bead beating. Samples were centrifuged for 1 min at 15,000 rcf, with 200 µL supernatant transferred into 1 mL deep-well plates and purified according to the manufacturer's instructions.

16S rRNA gene sequencing

The V4 region of the 16S rRNA gene was amplified using primers targeting 515F/806R regions (**Table S3**). The reaction mix was 0.45 µL DMSO, 0.0045 µL SYBR Green I 10x diluted in DMSO to 1000x, KAPA HiFi PCR kit (1.8 µL 5x KAPA HiFi Buffer, 0.27 µL 10 mM dNTPs, 0.18 µL KAPA HiFi polymerase), 0.045 µL of each amplification primer (final concentration 1 µM), 6.2055 µL nuclease-free water, and 1 µL DNA. A BioRad CFX 384 real-time PCR instrument amplified four 10-fold serial dilutions of DNA with the following parameters: 5 min 95°C, 20x (20 sec 98°C, 15 sec 55°C, 60 sec 72°C), hold 4°C. Non-plateaued individual sample dilutions were selected for indexing PCR. KAPA HiFi PCR kit was used with: 4 µL 5x KAPA HiFi Buffer, 0.6 µL 10 mM dNTPs, 1 µL DMSO, 0.4 µL KAPA HiFi polymerase, 4 µL indexing primer, 10 µL of 100-fold diluted primary PCR reaction. Secondary PCR amplification parameters were identical to Primary PCR. Amplicons were quantified with PicoGreen according to manufacturer's instructions, equimolar pooled, and gel purified (QIAquick Gel Extraction Kit). Libraries were quantified with KAPA Library Quantification Kit for Illumina Platforms according to the manufacturer's instructions, spiked with 15% PhiX, and sequenced on an Illumina MiSeqV3 instrument. Primers and adapters were removed using the cutadapt trim-paired command in QIIME2 (v2020.11) *(44)*. Sequences underwent trimming to 220 bp (forward) or 150 bp (reverse), quality filtering, denoising, and chimera filtering using dada2 (v1.18.0) with QIIME2 command denoise-paired *(45)*. Sequence length was filtered to 250-255 bp with QIIME2 command feature-table filter-seqs. Taxonomy was assigned to amplicon sequence variants (ASVs) using the SILVA v138 database *(46)*. Sequence variants not present in >3 samples with ≥10 reads were removed from downstream analysis.

16S rRNA gene analysis

Alpha diversity metrics were computed with Phyloseq command estimate_richness *(47)*. Differential alpha diversity was calculated with mixed effects model Diversity ~ Day + 1|Patient with the nlme (v3.1-164) command lme. ASV relative abundances were central log ratio (CLR)-transformed prior to further analysis. Principal coordinate analysis (PCoA) was performed with command prcomp (CLR-Euclidean ordination). PERMANOVA was performed using vegan (v2.6-4) commands vegdist (CLR-Euclidean ordination) and adonis2 *(48)*, with Patient as a strata. Differential abundance was calculated using mixed effects model Abundance ~ Day + 1|Patient, followed by false discovery rate (FDR) correction with R command p.adjust, with FDR < 0.2 called as significant. ASV phylogenetic tree construction was performed with QIIME2 command phylogeny align-to-tree-mafft-fasttree. Line plots were plotted using ggplot2 (v3.5.1) command geom_smooth with LOESS regression *(49)*.

Metagenomic sequencing

Shotgun libraries were prepared using the Illumina DNA Prep Tagmentation kit according to the manufacturer protocol. Libraries were assessed with PicoGreen and TapeStation 4200 (Agilent) for quantity and quality checks. Paired end libraries were sequenced using S1 flow cells on Illumina NovaSeq 6000 platforms. Demultiplexed reads underwent adapter trimming and quality filtering with FastP (v0.23.2) *(50)* and host read removal by mapping to human genome (GRCh38) with BMTagger (v3.101) *(51)*. Genome equivalents were quantified with microbeCensus (v1.1.1) *(52)*. Taxonomy was annotated with MetaPhlAn 4 *(53)*. Genes were annotated with HUMAnN 3.0 *(54)*, with UniRef90 families further mapped to KEGG Ortholog and Enzyme Class.

Metagenomic analysis

Gene abundances were normalized to reads per kilobase per genome equivalent using microbeCensus values prior to downstream analysis *(52)*. PCA was performed with command prcomp (CLR-Euclidean ordination). PERMANOVA was performed using vegan commands vegdist (CLR-Euclidean ordination) and adonis2 *(48)*, with Patient as a strata. Differential abundance was calculated with mixed effects model Abundance ~ Day + 1|Patient using the nlme command lme, followed by FDR correction, with FDR < 0.2 called as significant. Gene set enrichment analysis was performed on significant genes using clusterProfiler (v4.6.2) command enrichKEGG with a q-value cutoff of 0.2 *(55)*. Line plots were plotted using ggplot2 command geom_smooth with LOESS regression *(49)*.

Generation of *ex vivo* communities

Three patients from Cohort A with variable Baseline vs C1D7 diversity were selected for *ex vivo* communities. Brain Heart Infusion supplemented with L-cysteine hydrochloride (0.05% w/v), hemin (5 µg/ml), and vitamin K (1 µg/ml), termed BHI+, was used as media. 100 mg baseline stool from each patient was thawed and added anaerobically to 1 mL BHI+, vortexed for 1 min, and incubated 5 min at RT to allow debris to settle. 500 µL supernatant ("fecal slurry") was transferred to a new tube. 5-FU was dissolved in dimethylsulfoxide, supplemented at 1% (v/v) in BHI+ media and assayed at 50 ug/mL. 1% DMSO was added to BHI+ for CAP and vehicle groups; CAP was directly resuspended in this media and assayed at 5 mg/mL. 5 µL fecal slurry was inoculated in sextuplicate into 195 µL of media ± drug in a 96-well plate, with negative control wells to confirm media sterility. Plates were covered with BreathEasy covers and incubated at 37°C for 48 hr in a Gen5 plate reader, with 1 min linear shake prior to OD_{600} readings every 15 min. Plates were removed from plate reader and spun at 3000 rpm for 30 min, followed by supernatant ("spent media") transfer to a new plate.

Liquid chromatography-triple quadrupole mass spectrometry (LC–MS/MS) quantification of 5-FU from *ex vivo* communities

Quantification was performed using a validated 5-FU quantification protocol *(9)*. Briefly, spent media was thawed on ice. 50 µL spent media was dissolved in 150 µL water and 800 µL organic phase (50% ACN, 50% MeOH). A standard curve was generated by dissolving serial dilutions of 5-FU in DMSO into BHI+. 10 µL of 10 µg/ml 5-fluorouracil-^{13}C,$^{15}N_2$ internal standard was spiked into all samples. Samples were vortexed 5 min and incubated on ice for 30 min. Extraction mixture was spun down at 15000 rcf for 20 min. 250 µL extraction supernatant was dried in speed vac and resuspended in 200 µL of 10% ACN in water for injection. Samples were loaded into a Synergi column on a SCIEX Triple Quad 7500 instrument with a linear ion QTRAP. Chromatographic separation was achieved using a Phenomenex Synergi column 4 µM Fusion RP-80 (50 × 2 mm) at 35 °C. The mobile phase was methanol + 0.1% formic acid (A) and HPLC-grade water + 0.1% formic acid (B). A flow rate of 0.4 ml/min was used for the following gradient elution profile: 0% B at 0-2 min, gradient to 100% B from 2 to 5.9 min, gradient to 0% B at 5.9-6 min. The autosampler was maintained at 4 °C. Eluate from the column was ionized in the LC-MS/MS using an electrospray ionization source in positive polarity. Peak areas were

calculated using built-in SCIEX OS software. 5-FU peak area was normalized to the internal standard, with concentration calculated based on the 5-FU standard curve (Pearson $R^2 = 1.00$).

Mouse studies

All animal experiments were conducted under protocol AN200526 approved by the UCSF Institutional Animal Care and Use Committee. GF C57BL/6J mice were born at UCSF; specific pathogen free (SPF) C57BL6/J mice were purchased from Jackson Laboratory. Diets were provided *ad libitum*, with standard chow diet (LabDiet 5058) in the SPF facility and standard autoclaved chow diet (LabDiet 5021) in the gnotobiotic facility. Mouse age is reported in **Table S2**. Mice were housed at temperatures ranging from 67 to 74 °F and humidity ranging from 30 to 70% in light/dark cycle 12h/12h. GF mice were maintained within the UCSF Gnotobiotic Core Facility. Stool pellets from the Gnotobiotic Core Facility were screened every 2 weeks by culture and qPCR, whenever mice were transferred between isolators, and at the beginning and end of each experiment using V4_515F_Gnoto/V4_806R_Gnoto universal primers (**Table S3**).

CAP dosing in murine models

Buffer was prepared by dissolving 964 mg sodium citrate dihydrate and 139 mg of citric acid into 90 mL deionized water (DI), adjusting pH to 6.0 with HCl or NaOH, adding 5 g gum arabic, bringing final volume to 100 mL, and autoclaving for 20 min. CAP solution was prepared fresh daily (SPF experiments) or weekly (gnotobiotic experiments) by dissolving CAP into the buffer with continuous agitation and heating. Mice were given a single CAP bolus daily by oral gavage. CAP was dosed by body weight, with CAP quantity determined such that 200 µL solution contained the total CAP dose (1100 or 1500 mg/kg) for the largest mouse. Gavage needles were rinsed with DI in between each mouse, with different needles for each experimental group.

Establishment of CAP toxicity experiment

20 mice were gavaged with 1500 mg/kg CAP (n = 12) or 200 µL buffer ($n = 8$) once daily. Half the mice were sacrificed at Day 4, with remaining mice sacrificed at Day 12. Endpoint small intestine, cecum, and colon contents were collected. 5 metrics were used to assess toxicity. (1) *Weight loss and survival time*. Mice were weighed daily and sacrificed at 15% weight loss ("survival time") or at experimental endpoint, whichever came first. (2) *Anatomic measurements*. Mouse colon length, small intestine length, spleen weight, and gonadal fat pad weight were measured. (3) *Body composition*. Mouse body composition was measured at Days 0, 4, and 12 by EchoMRI with 1 primary accumulation. (4) *Lipocalin-2 ELISA*. Enzyme-linked immunosorbent assay was performed with Mouse Lipocalin-2/NGAL DuoSet ELISA kit using the manufacturer's protocol with the following modifications: (a) preweighed colon contents (50-100 mg) were combined with 1 mL PBS + 0.1% Tween 20 and vortexed for 20 min, then centrifuged for 10 min at 4°C and 12,000 rcf. For sample wells, 20 µL of extracted sample was added to 100 µL of reagent diluent and 6-fold serially diluted. (b) For standard wells, 125 pg/mL mouse lipocalin-2 standard with 2-fold serial dilutions was used, with two blank wells. (c) Absolute concentrations were calculated with linear fit to a log-log plot of mouse Lcn-2 concentration vs OD. (5) *Hand-foot syndrome*. Thermal hind paw hyperalgesia was measured as

described in *(20)*. Briefly, mice were placed on a 52°C hotplate and latency to rear paw lick, rear paw flick, or jump was recorded.

Broad-spectrum antibiotic CAP toxicity experiment

Antibiotic (AVNM) or Vehicle (Veh) water was prepared fresh weekly from autoclaved tap water supplemented with sucrose (0.5 g/L sucrose) ± antibiotics (1g/L ampicillin, 0.5g/L vancomycin, 1 g/L neomycin, 0.5 g/L metronidazole), followed by 0.2 µm filter sterilization. 24 mice were treated *ad libitum* with AVNM (n = 12) or Veh (n = 12) water for the duration of the experiment. After 1 week of antibiotics, mice were treated with 1500 mg/kg CAP daily for 2 weeks. Weight was measured daily and stool was taken at Days -7, 0, 3, 5 (relative to CAP start). Endpoint small intestine, cecum, and colon contents were collected. Endpoint cecal contents weight and gonadal fat pad weight were measured. To assess bacterial load, fecal slurries were generated by adding 100 mg Day 0 stool into 1 mL BHI+, vortexing for 1 min, and allowing fecal debris to settle for 5 min. 10 µL of supernatant was 10x serially diluted in BHI+, with 2.5 µL of each dilution spotted on BHI+ agar plates and incubated at 37°C for 5 days to quantify colony forming units (CFUs). All stool work was performed anaerobically.

Germ-free vs conventional microbiota CAP toxicity experiment

To generate CONV-D mice, cecal contents from a single SPF donor was resuspended in 10% BHI+ aerobically and passed through a 100 µm filter, with 200 µL administered to GF mice followed by a 1 week engraftment period. CONV-R (n = 8), CONV-D (n = 8), and GF (n = 8) mice were treated with 1100 mg/kg CAP daily for 2 weeks. Weight was measured daily. Endpoint small intestine contents, cecal contents, colon contents, and large intestine length were collected for all mice, with endpoint small intestine length, spleen weight, cecal contents weight, and gonadal fat pad weight collected for CONV-D and GF mice.

preTA CAP rescue experiment

Streptomycin water was prepared fresh weekly from autoclaved tap water supplemented with 5 g/L streptomycin, followed by 0.2 µm filter sterilization. 32 mice were treated *ad libitum* with streptomycin water for the duration of the experiment. Overnight cultures of engineered *E. coli* strains (*E. coli* Δ*preTA* and *E. coli preTA*$^{++}$) were pelleted by centrifugation, washed with an equal volume of sterile 0.85% saline, pelleted by centrifugation, and resuspended in 1:10 sterile saline. Mice were gavaged with 200 µl bacterial suspension (n = 16 *E. coli* Δ*preTA*, n = 16 *E. coli preTA*$^{++}$) by gavage following 1 day on strep water. One day post-colonization ("Day 0"), mice began 2 weeks of treatment with 1500 mg/kg CAP daily. Weight was measured daily and stool was taken at Days -1, 0, 4, 7. Endpoint small intestine, cecum, and colon contents were collected. Fecal slurries were generated by anaerobically adding 100 mg Day 0 stool into 1 mL LB + strep, vortexing 1 min, and allowing fecal debris to settle for 5 min. 10 µL of supernatant was 10-fold serially diluted in LB + strep, with 2.5 µL of each dilution spotted on EMB agar plates and incubated anaerobically at 37°C for 2 days to quantify *E. coli* CFUs.

Gnotobiotic *preTA* CAP rescue experiment

Overnight cultures of engineered *E. coli* strains (*E. coli* Δ*preTA* and *E. coli preTA*$^{++}$) were pelleted by centrifugation, washed with an equal volume of sterile 0.85% saline, pelleted by centrifugation again and resuspended in 1:10 sterile saline. Mice were gavaged with 200 µl bacterial suspension or saline only (n = 6 *E. coli* Δ*preTA*, n = 6 *E. coli preTA*$^{++}$, n = 6 "mock"). One week post-colonization, stool was collected and mice began 2 weeks of treatment with 1500 mg/kg CAP daily, with weight measured daily. Endpoint small intestine length and colon length were measured. Endpoint *E. coli* CFUs from Day 0 stool were quantified by culturing on MacConkey Agar as described previously *(9)*. For group comparisons, Δ*preTA* and mock colonized mice were binned together into "mock/Δ*preTA*" (both contain no *preTA*).

Gnotobiotic humanization CAP toxicity experiments

Two independent experiments were conducted. For each experiment, two donors with variable baseline *preTA* were selected to humanize 16 gnotobiotic mice (n = 8 per donor; 1 isolator per donor). Fecal slurries were generated anaerobically by adding 100 mg stool to 2 mL PBS, vortexing, and letting the mixture settle for 5 min. 1.5 mL of supernatant ("fecal slurry") was transferred to a new tube on ice. 100 µL fecal slurry was orally gavaged into each mouse, with the researcher blinded to colonization group. One week post-colonization, baseline stool was collected and mice began 2 weeks of treatment with 1500 mg/kg CAP daily. Weight was measured daily. Endpoint stool, small intestine contents, cecal contents, colon contents, colon length, spleen weight, and gonadal fat pad weights were collected. Baseline stool was subjected to metagenomic sequencing to assess *preTA* status. For group comparisons, mice with no detected K17722/K17723 were called "*preTA* low", with others called *"preTA* high." Where stool was not evaluable (1/32 mice), mice were called as the *preTA* level of their cagemates.

Statistical analysis

Statistical analysis was performed in R (v4.2.1) *(56)*, with plots generated using ggplot2 (v3.5.1) and ggpubr (v0.6.0) *(49, 57)*. All statistical tests are specified in the text or figure legends where used, with core tests summarized here. Linear mixed-effects models with day as a fixed effect and patient as a random effect were used to identify statistically significant changes in alpha diversity, beta diversity, taxa, and genes with respect to time. For differential mixed-effects analyses, samples prior to Day 0 (1st day of treatment) were set to Day 0. Diversity, taxa, and genes were plotted with respect to time by LOESS regression with standard error shaded; patients where the taxa/gene of interest was not detected in any samples were excluded from these plots. PERMANOVA testing with treatment and patient as effects and patient as a strata was used to test for compositional differences in taxa and genes (CLR-Euclidean ordination). Comparisons between two groups were performed with Mann-Whitney U test or ANOVA. Comparisons between three groups were performed with Kruskal-Wallis testing. Two-way ANOVA was used to identify significant group differences in mouse weight with respect to time. Mouse weights are plotted as mean with standard error bars; days after the first mouse sacrifice due to 15% weight loss are excluded from these plots. Spearman correlation was used to identify significant relationships between continuous variables. Survival distributions were compared with the Mantel-Cox test. pROC (v1.18.5) command roc was for calculating sensitivity, specificity, and AUC *(58)*. Significance was determined as p-value < 0.05 (individual tests) or Benjamini-Hochberg FDR < 0.2 (multiple hypothesis correction of taxa/genes).

List of Supplementary Materials

Figs. S1-S9

Tables S1-S3

Data Files S1-S5

References

1. P. Y. Muller, M. N. Milton, The determination and interpretation of the therapeutic index in drug development. *Nat. Rev. Drug Discov.* **11**, 751–761 (2012).

2. Q. Ma, A. Y. H. Lu, Pharmacogenetics, pharmacogenomics, and individualized medicine. *Pharmacol. Rev.* **63**, 437–459 (2011).

3. B. Tamraz, A. P. Venook, DPYD Pharmacogenetics: To Opt-in or to Opt-out. *JCO Oncol Pract* , OP2400255 (2024).

4. M. Zimmermann, M. Zimmermann-Kogadeeva, R. Wegmann, A. L. Goodman, Mapping human microbiome drug metabolism by gut bacteria and their genes. *Nature* **570**, 462–467 (2019).

5. B. Javdan, J. G. Lopez, P. Chankhamjon, Y.-C. J. Lee, R. Hull, Q. Wu, X. Wang, S. Chatterjee, M. S. Donia, Personalized Mapping of Drug Metabolism by the Human Gut Microbiome. *Cell* **181**, 1661–1679.e22 (2020).

6. K. D. Miller, L. Nogueira, T. Devasia, A. B. Mariotto, K. R. Yabroff, A. Jemal, J. Kramer, R. L. Siegel, Cancer treatment and survivorship statistics, 2022. *CA Cancer J. Clin.* **72**, 409–436 (2022).

7. M. W. Saif, N. A. Katirtzoglou, K. N. Syrigos, Capecitabine: an overview of the side effects and their management. *Anticancer Drugs* **19**, 447–464 (2008).

8. D. R. Budman, Capecitabine. *Invest. New Drugs* **18**, 355–363 (2000).

9. P. Spanogiannopoulos, T. S. Kyaw, B. G. H. Guthrie, P. H. Bradley, J. V. Lee, J. Melamed, Y. N. A. Malig, K. N. Lam, D. Gempis, M. Sandy, Others, Host and gut bacteria share metabolic pathways for anti-cancer drug metabolism. *Nature microbiology* **7**, 1605–1620 (2022).

10. D. Liu, L.-S. Xie, S. Lian, K. Li, Y. Yang, W.-Z. Wang, S. Hu, S.-J. Liu, C. Liu, Z. He, Anaerostipes hadrus, a butyrate-producing bacterium capable of metabolizing 5-fluorouracil. *mSphere* , e0081623 (2024).

11. C. A. T. C. Lunenburg, L. M. Henricks, H.-J. Guchelaar, J. J. Swen, M. J. Deenen, J. H. M. Schellens, H. Gelderblom, Prospective DPYD genotyping to reduce the risk of fluoropyrimidine-induced severe toxicity: Ready for prime time. *Eur. J. Cancer* **54**, 40–48 (2016).

12. D. Rosmarin, C. Palles, D. Church, E. Domingo, A. Jones, E. Johnstone, H. Wang, S. Love, P. Julier, C. Scudder, G. Nicholson, A. Gonzalez-Neira, M. Martin, D. Sargent, E. Green, H. McLeod, U. M. Zanger, M. Schwab, M. Braun, M. Seymour, L. Thompson, B. Lacas, V. Boige, N. Ribelles, S. Afzal, H. Enghusen, S. A. Jensen, M.-C. Etienne-Grimaldi, G. Milano, M. Wadelius, B. Glimelius, H. Garmo, M. Gusella, T. Lecomte, P. Laurent-Puig, E. Martinez-Balibrea, R. Sharma, J. Garcia-Foncillas, Z. Kleibl, A. Morel, J.-P. Pignon, R. Midgley, D. Kerr, I. Tomlinson, Genetic markers of toxicity from capecitabine and other fluorouracil-based regimens: investigation in the QUASAR2 study, systematic review, and meta-analysis. *J. Clin. Oncol.* **32**, 1031–1039 (2014).

13. B. A. W. Jacobs, M. J. Deenen, M. Joerger, H. Rosing, N. de Vries, D. Meulendijks, A. Cats, J. H. Beijnen, J. H. M. Schellens, A. D. R. Huitema, Pharmacokinetics of Capecitabine and Four Metabolites in a Heterogeneous Population of Cancer Patients: A Comprehensive Analysis. *CPT Pharmacometrics Syst Pharmacol* **8**, 940–950 (2019).

14. B. A. Jennings, Y. K. Loke, J. Skinner, M. Keane, G. S. Chu, R. Turner, D. Epurescu, A. Barrett, G. Willis, Evaluating predictive pharmacogenetic signatures of adverse events in colorectal cancer patients treated with fluoropyrimidines. *PLoS One* **8**, e78053 (2013).

15. S. Piawah, T. S. Kyaw, K. Trepka, A. L. Stewart, R. V. Mora, D. Stanfield, K. Levine, E. L. Van Blarigan, A. Venook, P. J. Turnbaugh, T. Nguyen, C. E. Atreya, Associations between the Gut Microbiota, Race, and Ethnicity of Patients with Colorectal Cancer: A Pilot and Feasibility Study. *Cancers* **15** (2023), doi:10.3390/cancers15184546.

16. R. Aarnoutse, J. Ziemons, J. de Vos-Geelen, L. Valkenburg-van Iersel, A. C. L. Wildeboer, A. Vievermans, G.-J. M. Creemers, A. Baars, H. J. H. M. J. Vestjens, G. N. Le, D. J. M. Barnett, S.

S. Rensen, J. Penders, M. L. Smidt, The Role of Intestinal Microbiota in Metastatic Colorectal Cancer Patients Treated With Capecitabine. *Clin. Colorectal Cancer* **21**, e87–e97 (2022).

17. G. A. O'Donovan, J. Neuhard, Pyrimidine metabolism in microorganisms. *Bacteriol. Rev.* **34**, 278–343 (1970).

18. B. Rosener, S. Sayin, P. O. Oluoch, A. P. García González, H. Mori, A. J. Walhout, A. Mitchell, Evolved bacterial resistance against fluoropyrimidines can lower chemotherapy impact in the Caenorhabditis elegans host. *Elife* **9** (2020), doi:10.7554/eLife.59831.

19. A. B. Nair, S. Jacob, A simple practice guide for dose conversion between animals and human. *J. Basic Clin. Physiol. Pharmacol.* **7**, 27–31 (2016).

20. B. Yang, X. Xie, D. Lv, J. Hu, Y. Chen, Z. Wu, S. Luo, S. Zhang, Capecitabine induces hand-foot syndrome through elevated thymidine phosphorylase-mediated locoregional toxicity and GSDME-driven pyroptosis that can be relieved by tipiracil. *Br. J. Cancer* **128**, 219–231 (2023).

21. T. A. Suzuki, J. L. Fitzstevens, V. T. Schmidt, H. Enav, K. E. Huus, M. Mbong Ngwese, A. Grießhammer, A. Pfleiderer, B. R. Adegbite, J. F. Zinsou, M. Esen, T. P. Velavan, A. A. Adegnika, L. H. Song, T. D. Spector, A. L. Muehlbauer, N. Marchi, H. Kang, L. Maier, R. Blekhman, L. Ségurel, G. Ko, N. D. Youngblut, P. Kremsner, R. E. Ley, Codiversification of gut microbiota with humans. *Science* **377**, 1328–1332 (2022).

22. K. A. Lee, A. M. Thomas, L. A. Bolte, J. R. Björk, L. K. de Ruijter, F. Armanini, F. Asnicar, A. Blanco-Miguez, R. Board, N. Calbet-Llopart, L. Derosa, N. Dhomen, K. Brooks, M. Harland, M. Harries, E. R. Leeming, P. Lorigan, P. Manghi, R. Marais, J. Newton-Bishop, L. Nezi, F. Pinto, M. Potrony, S. Puig, P. Serra-Bellver, H. M. Shaw, S. Tamburini, S. Valpione, A. Vijay, L. Waldron, L. Zitvogel, M. Zolfo, E. G. E. de Vries, P. Nathan, R. S. N. Fehrmann, V. Bataille, G. A. P. Hospers, T. D. Spector, R. K. Weersma, N. Segata, Cross-cohort gut microbiome associations with immune checkpoint inhibitor response in advanced melanoma. *Nat. Med.* **28**, 535–544 (2022).

23. Y. Kawasaki, K. Kakimoto, Y. Tanaka, H. Shimizu, K. Nishida, K. Numa, N. Kinoshita, Y. Tatsumi, K. Nakazawa, R. Koshiba, Y. Hirata, K. Ota, N. Sakiyama, T. Terazawa, T. Takeuchi, T. Miyazaki, M. Goto, H. Yokota, Y. Makizaki, Y. Tanaka, S. Nakajima, H. Ohno, K. Higuchi, S. Nakamura, H. Nishikawa, Relationship between Chemotherapy-Induced Diarrhea and Intestinal Microbiome Composition. *Digestion* **104**, 357–369 (2023).

24. Y. Gao, P. Xu, D. Sun, Y. Jiang, X.-L. Lin, T. Han, J. Yu, C. Sheng, H. Chen, J. Hong, Y. Chen, X.-Y. Xiao, J.-Y. Fang, Faecalibacterium prausnitzii Abrogates Intestinal Toxicity and Promotes Tumor Immunity to Increase the Efficacy of Dual CTLA4 and PD-1 Checkpoint Blockade. *Cancer Res.* **83**, 3710–3725 (2023).

25. A. Gunjur, Y. Shao, T. Rozday, O. Klein, A. Mu, B. W. Haak, B. Markman, D. Kee, M. S. Carlino, C. Underhill, S. Frentzas, M. Michael, B. Gao, J. Palmer, J. Cebon, A. Behren, D. J. Adams, T. D. Lawley, A gut microbial signature for combination immune checkpoint blockade across cancer types. *Nat. Med.* **30**, 797–809 (2024).

26. V. G. Lewis, M. P. Ween, C. A. McDevitt, The role of ATP-binding cassette transporters in bacterial pathogenicity. *Protoplasma* **249**, 919–942 (2012).

27. J. Jovel, A. Nimaga, T. Jordan, S. O'Keefe, J. Patterson, A. Thiesen, N. Hotte, M. Bording-Jorgensen, S. Subedi, J. Hamilton, E. J. Carpenter, B. Lauga, S. Elahi, K. L. Madsen, G. K.-S. Wong, A. L. Mason, Metagenomics Versus Metatranscriptomics of the Murine Gut Microbiome for Assessing Microbial Metabolism During Inflammation. *Front. Microbiol.* **13**, 829378 (2022).

28. H. Imai, K. Saijo, K. Komine, Y. Yoshida, K. Sasaki, A. Suzuki, K. Ouchi, M. Takahashi, S. Takahashi, H. Shirota, M. Takahashi, C. Ishioka, Antibiotics Improve the Treatment Efficacy of Oxaliplatin-Based but Not Irinotecan-Based Therapy in Advanced Colorectal Cancer Patients. *J. Oncol.* **2020**, 1701326 (2020).

29. K. Takasuna, T. Hagiwara, M. Hirohashi, M. Kato, M. Nomura, E. Nagai, T. Yokoi, T. Kamataki, Inhibition of intestinal microflora beta-glucuronidase modifies the distribution of the active metabolite of the antitumor agent, irinotecan hydrochloride (CPT-11) in rats. *Cancer Chemother. Pharmacol.* **42**, 280–286 (1998).

30. D. Flieger, C. Klassert, S. Hainke, R. Keller, R. Kleinschmidt, W. Fischbach, Phase II clinical trial for prevention of delayed diarrhea with cholestyramine/levofloxacin in the second-line treatment with irinotecan biweekly in patients with metastatic colorectal carcinoma. *Oncology* **72**, 10–16 (2007).

31. R.-H. Xu, K. Muro, S. Morita, S. Iwasa, S. W. Han, W. Wang, M. Kotaka, M. Nakamura, J. B. Ahn, Y.-H. Deng, T. Kato, S.-H. Cho, Y. Ba, H. Matsuoka, K.-W. Lee, T. Zhang, Y. Yamada, J. Sakamoto, Y. S. Park, T. W. Kim, Modified XELIRI (capecitabine plus irinotecan) versus FOLFIRI (leucovorin, fluorouracil, and irinotecan), both either with or without bevacizumab, as second-line therapy for metastatic colorectal cancer (AXEPT): a multicentre, open-label, randomised, non-inferiority, phase 3 trial. *Lancet Oncol.* **19**, 660–671 (2018).

32. Role of dihydropyrimidine dehydrogenase deficiency in systemic fluoropyrimidine-related toxicity (available at https://www.medsafe.govt.nz/profs/PUArticles/March2023/Role-of-DPD-deficiency-in-systemic-fluoropyrimidine-related-toxicity.html).

33. W. H. Gmeiner, A narrative review of genetic factors affecting fluoropyrimidine toxicity. *Precis Cancer Med* **4** (2021), doi:10.21037/pcm-21-17.

34. J. A. Seltzer, N. A. Friedman, J. Hardin, H. Galust, F. L. Cantrell, A. Minns, Oral Capecitabine Exposures and Use of Uridine Triacetate: A 20-Year Retrospective Analysis. *Clin. Drug Investig.* **43**, 359–363 (2023).

35. C.-W. Chang, H.-C. Lee, L.-H. Li, J.-S. Chiang Chiau, T.-E. Wang, W.-H. Chuang, M.-J. Chen, H.-Y. Wang, S.-C. Shih, C.-Y. Liu, T.-H. Tsai, Y.-J. Chen, Fecal Microbiota Transplantation Prevents Intestinal Injury, Upregulation of Toll-Like Receptors, and 5-Fluorouracil/Oxaliplatin-Induced Toxicity in Colorectal Cancer. *Int. J. Mol. Sci.* **21** (2020), doi:10.3390/ijms21020386.

36. P. Osterlund, T. Ruotsalainen, R. Korpela, M. Saxelin, A. Ollus, P. Valta, M. Kouri, I. Elomaa, H. Joensuu, Lactobacillus supplementation for diarrhoea related to chemotherapy of colorectal cancer: a randomised study. *Br. J. Cancer* **97**, 1028–1034 (2007).

37. H. Zeng, H. Yu, L. Lu, D. Jain, M. S. Kidd, M. W. Saif, S. J. Chanock, P. Hartge, PanScan Consortium, H. A. Risch, Genetic effects and modifiers of radiotherapy and chemotherapy on survival in pancreatic cancer. *Pancreas* **40**, 657–663 (2011).

38. A. B. Van Kuilenburg, P. Vreken, N. G. Abeling, H. D. Bakker, R. Meinsma, H. Van Lenthe, R. A. De Abreu, J. A. Smeitink, H. Kayserili, M. Y. Apak, E. Christensen, I. Holopainen, K. Pulkki, D. Riva, G. Botteon, E. Holme, M. Tulinius, W. J. Kleijer, F. A. Beemer, M. Duran, K. E. Niezen-Koning, G. P. Smit, C. Jakobs, L. M. Smit, A. H. Van Gennip, Genotype and phenotype in patients with dihydropyrimidine dehydrogenase deficiency. *Hum. Genet.* **104**, 1–9 (1999).

39. J. E. Knikman, M. Lopez-Yurda, D. Meulendijks, M. J. Deenen, J. H. M. Schellens, J. Beijnen, A. Cats, H.-J. Guchelaar, A Nomogram to Predict Severe Toxicity in DPYD Wild-Type Patients Treated With Capecitabine-Based Anticancer Regimens. *Clin. Pharmacol. Ther.* **115**, 269–277 (2024).

40. C. Palles, S. Fotheringham, L. Chegwidden, M. Lucas, R. Kerr, G. Mozolowski, D. Rosmarin, J. C. Taylor, I. Tomlinson, D. Kerr, An Evaluation of the Diagnostic Accuracy of a Panel of Variants in DPYD and a Single Variant in ENOSF1 for Predicting Common Capecitabine Related Toxicities. *Cancers* **13** (2021), doi:10.3390/cancers13071497.

41. K. Ota, T. Takeuchi, Y. Kojima, S. Harada, H. Ozaki, N. Sugawara, Y. Hirata, T. Yamaguchi, T. Terazawa, K. Kakimoto, T. Kii, M. Goto, K. Higuchi, Fluoropyrimidine-induced intestinal mucosal injury is associated with the severity of chemotherapy-related diarrhea. *Scand. J. Gastroenterol.* **54**, 227–232 (2019).

42. E. Van Cutsem, P. M. Hoff, P. Harper, R. M. Bukowski, D. Cunningham, P. Dufour, U. Graeven, J. Lokich, S. Madajewicz, J. A. Maroun, J. L. Marshall, E. P. Mitchell, G. Perez-Manga, P. Rougier, W. Schmiegel, J. Schoelmerich, A. Sobrero, R. L. Schilsky, Oral capecitabine vs intravenous 5-fluorouracil and leucovorin: integrated efficacy data and novel analyses from two large, randomised, phase III trials. *Br. J. Cancer* **90**, 1190–1197 (2004).

43. N. Fidelman, C. E. Atreya, M. Griffith, M. A. Milloy, J. Carnevale, P. Cinar, A. P. Venook, K. Van Loon, Phase I prospective trial of TAS-102 (trifluridine and tipiracil) and radioembolization with 90Y resin microspheres for chemo-refractory colorectal liver metastases. *BMC Cancer* **22**, 1307 (2022).

44. M. Hall, R. G. Beiko, in *Microbiome Analysis: Methods and Protocols*, R. G. Beiko, W. Hsiao, J. Parkinson, Eds. (Springer New York, New York, NY, 2018), pp. 113–129.

45. B. J. Callahan, P. J. McMurdie, M. J. Rosen, A. W. Han, A. J. A. Johnson, S. P. Holmes, DADA2: High-resolution sample inference from Illumina amplicon data. *Nat. Methods* **13**, 581–583 (2016).

46. C. Quast, E. Pruesse, P. Yilmaz, J. Gerken, T. Schweer, P. Yarza, J. Peplies, F. O. Glöckner,

The SILVA ribosomal RNA gene database project: improved data processing and web-based tools. *Nucleic Acids Res.* **41**, D590–6 (2013).

47. P. J. McMurdie, S. Holmes, phyloseq: an R package for reproducible interactive analysis and graphics of microbiome census data. *PLoS One* **8**, e61217 (2013).

48. P. Dixon, VEGAN, a package of R functions for community ecology. *J. Veg. Sci.* **14**, 927–930 (2003).

49. L. Wilkinson, ggplot2: Elegant Graphics for Data Analysis by WICKHAM, H. *Biometrics* **67**, 678–679 (2011).

50. S. Chen, Y. Zhou, Y. Chen, J. Gu, fastp: an ultra-fast all-in-one FASTQ preprocessor. *Bioinformatics* **34**, i884–i890 (2018).

51. K. Rotmistrovsky, R. Agarwala, BMTagger: Best Match Tagger for removing human reads from metagenomics datasets. *NCBI/NLM, National Institutes of Health* .

52. S. Nayfach, K. S. Pollard, Average genome size estimation improves comparative metagenomics and sheds light on the functional ecology of the human microbiome. *Genome Biol.* **16**, 51 (2015).

53. A. Blanco-Míguez, F. Beghini, F. Cumbo, L. J. McIver, K. N. Thompson, M. Zolfo, P. Manghi, L. Dubois, K. D. Huang, A. M. Thomas, W. A. Nickols, G. Piccinno, E. Piperni, M. Punčochář, M. Valles-Colomer, A. Tett, F. Giordano, R. Davies, J. Wolf, S. E. Berry, T. D. Spector, E. A. Franzosa, E. Pasolli, F. Asnicar, C. Huttenhower, N. Segata, Extending and improving metagenomic taxonomic profiling with uncharacterized species using MetaPhlAn 4. *Nat. Biotechnol.* **41**, 1633–1644 (2023).

54. F. Beghini, L. J. McIver, A. Blanco-Míguez, L. Dubois, F. Asnicar, S. Maharjan, A. Mailyan, P. Manghi, M. Scholz, A. M. Thomas, M. Valles-Colomer, G. Weingart, Y. Zhang, M. Zolfo, C. Huttenhower, E. A. Franzosa, N. Segata, Integrating taxonomic, functional, and strain-level profiling of diverse microbial communities with bioBakery 3. *Elife* **10** (2021), doi:10.7554/eLife.65088.

55. G. Yu, L.-G. Wang, Y. Han, Q.-Y. He, clusterProfiler: an R package for comparing biological themes among gene clusters. *OMICS* **16**, 284–287 (2012).

56. R. Ihaka, R. Gentleman, R: A Language for Data Analysis and Graphics. *J. Comput. Graph. Stat.* **5**, 299–314 (1996).

57. A. Kassambara, Ggpubr: “ggplot2” based publication ready plots. *R package version* **0**, 2 (2018).

58. X. Robin, N. Turck, A. Hainard, N. Tiberti, F. Lisacek, J.-C. Sanchez, M. Müller, pROC: an open-source package for R and S+ to analyze and compare ROC curves. *BMC Bioinformatics* **12**, 77 (2011).

Acknowledgements

Gnotobiotic experiments were performed at the UCSF Gnotobiotics Core Facility. Sequencing was performed at Chan-Zuckerberg Biohub-San Francisco and the UCSF Center for Advanced Technology. Diagrams were created with Biorender.com.

Funding:

National Institutes of Health Grant F30CA257378 (TSK)

National Institutes of Health Grants R01HL122593, R01CA255116 (PJT)

Parkinson's Disease Foundation Grant PF-PRF-932695 (CAO)

Author contributions:

Conceptualization: KRT, WAK, TSK, CEA, EVB, PJT

Methodology: KRT, TSK, CN, CAO, VU, JAT, DD, PJT

Investigation: KRT, TSK, CAO, MDS, PS, DS

Visualization: KRT

Funding acquisition: WAK, AV, CEA, PJT

Project administration: WAK, PJT

Supervision: CAO, VU, CN, CEA, PJT

Writing – original draft: KRT, PJT

Writing – review & editing: All authors

Competing interests: W.A.K. has received research funding (institution) from Pfizer; there is no direct overlap with the current study. P.J.T. is on the scientific advisory boards of Pendulum, Seed and SNIPRbiome; there is no direct overlap between the current study and these consulting duties. C.E.A served on the scientific advisory board of Pionyr Immunotherapeutics and has received research funding (institution) from Bristol Meyer Squibb, Erasca, Gossamer Bio, Guardant Health, Kura Oncology, Merck and Novartis; there is no direct overlap with the current study. E.V.B. is on the medical advisory board for Fight CRC; there is no direct overlap with the current study. All other authors declare no competing interests.

Data and materials availability: This study did not generate new reagents. All code and data for generating figures is on GitHub at https://github.com/turnbaughlab/2024_Trepka_GO. The accession number for the sequencing data reported in this paper is NCBI Sequence Read Archive: TBD.

Figures

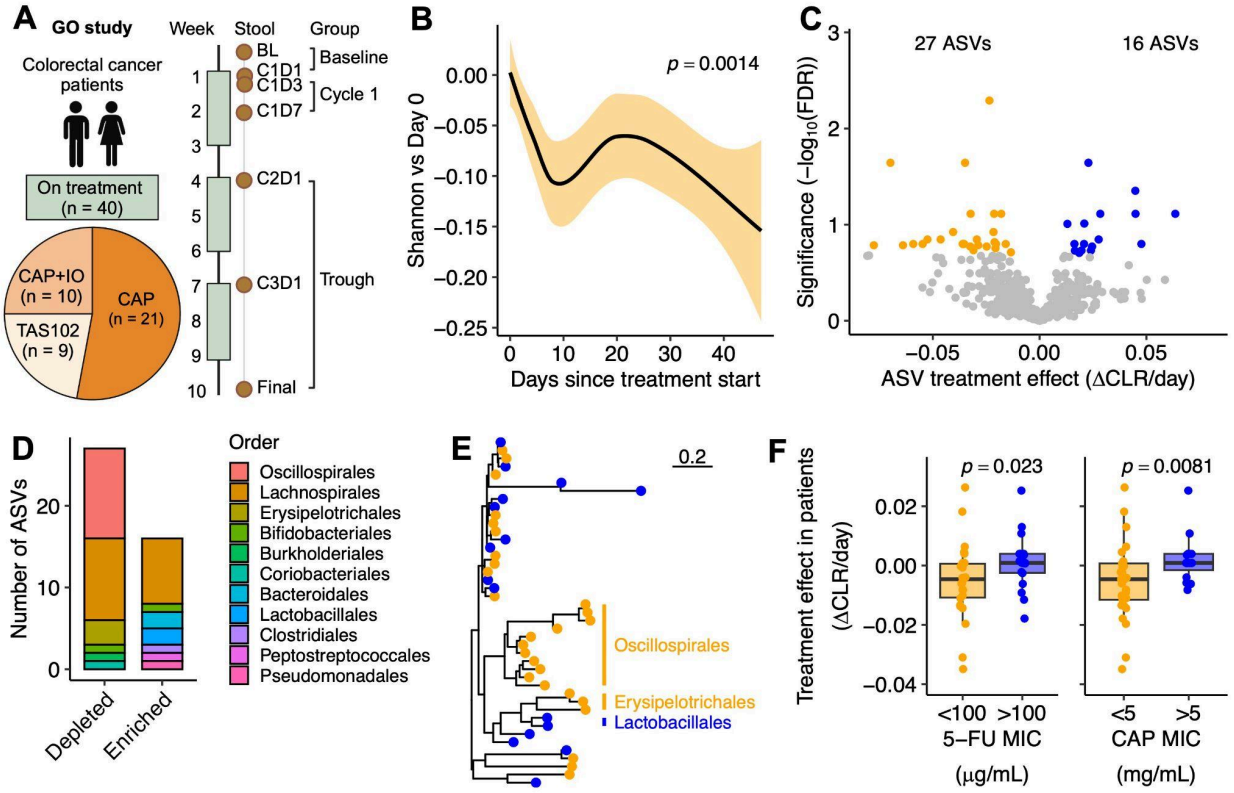

Figure 1: Oral fluoropyrimidine treatment impacts gut microbiome composition in colorectal cancer patients. (A) Gut microbiome and Oral fluoropyrimidine (GO) study design depicting patients treated with capecitabine (CAP), TAS-102, or combination CAP + immunotherapy (IO). **(B)** Change in alpha diversity during the study, normalized to baseline. *p*-value: mixed-effects model, Shannon ~ Day + 1|Patient. Solid line with shading represents LOESS interpolation mean±sem. **(C)** Volcano plot of microbial amplicon sequence variants (ASVs) with respect to treatment time. *p*-value: mixed-effects model, central log ratio (CLR)-transformed Abundance ~ Day + 1|Patient. Points represent enriched (blue) and depleted (orange) ASVs after treatment (false discovery rate (FDR) < 0.2). **(D)** Enriched and depleted ASV Order. **(E)** Phylogenetic tree of significantly differentially abundant ASVs, with labels for clades where treatment affected all clade members similarly (enriched (blue) or depleted (orange)). **(F)** Relationship between the impact of fluoropyrimidines on ASVs in patients and *in vitro*. *p*-value: one-sided Mann-Whitney U test.

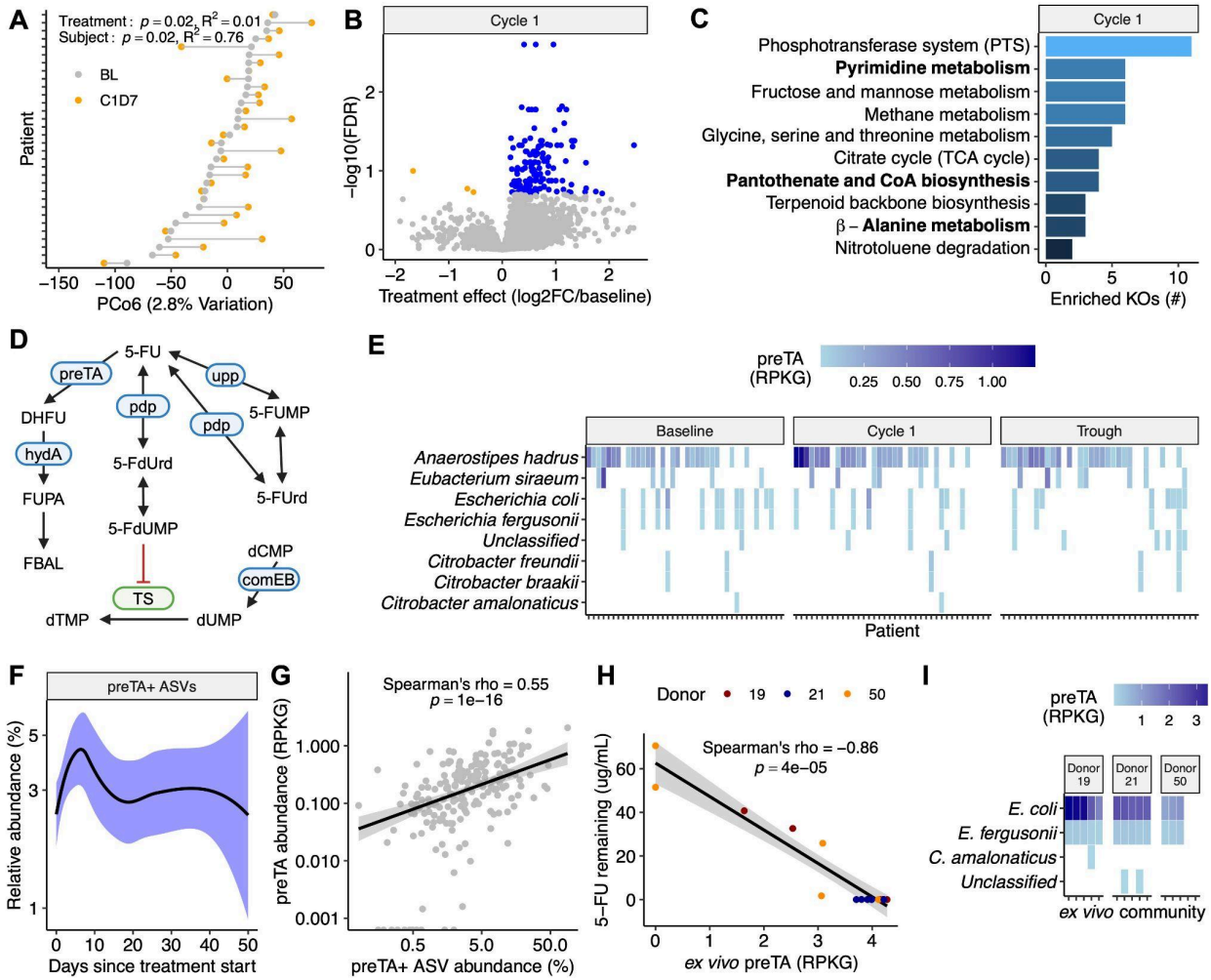
A
Treatment : p = 0.02, R2 = 0.01
Subject : p = 0.02, R2 = 0.76
BL
C1D7
Patient
PCo6 (2.8% Variation)
B
Cycle 1
−log10(FDR)
Treatment effect (log2FC/baseline)
C
Cycle 1
Phosphotransferase system (PTS)
Pyrimidine metabolism
Fructose and mannose metabolism
Methane metabolism
Glycine, serine and threonine metabolism
Citrate cycle (TCA cycle)
Pantothenate and CoA biosynthesis
Terpenoid backbone biosynthesis
β – Alanine metabolism
Nitrotoluene degradation
Enriched KOs (#)
D
5-FU
preTA
upp
DHFU
pdp
pdp
5-FUMP
hydA
5-FdUrd
FUPA
5-FUrd
5-FdUMP
FBAL
dCMP
comEB
TS
dTMP
dUMP
E
preTA (RPKG)
0.25 0.50 0.75 1.00
Baseline
Cycle 1
Trough
Anaerostipes hadrus
Eubacterium siraeum
Escherichia coli
Escherichia fergusonii
Unclassified
Citrobacter freundii
Citrobacter braakii
Citrobacter amalonaticus
Patient
F
preTA+ ASVs
Relative abundance (%)
Days since treatment start
G
Spearman's rho = 0.55
p = 1e−16
preTA abundance (RPKG)
preTA+ ASV abundance (%)
H
Donor 19 21 50
Spearman's rho = −0.86
p = 4e−05
5−FU remaining (ug/mL)
ex vivo preTA (RPKG)
I
preTA (RPKG)
1 2 3
Donor 19
Donor 21
Donor 50
E. coli
E. fergusonii
C. amalonaticus
Unclassified
ex vivo community

Figure 2: Oral fluoropyrimidine treatment selects for the bacterial drug metabolism gene *preTA*. (A) Reproducible shifts in gut microbial KEGG ortholog (KO) gene content are observed across study participants with BL and C1D7 samples (n = 32) on the sixth principal coordinate (PCo6) of Euclidean distances between central log ratio (CLR)-transformed RPKGs. p-value: PERMANOVA with Patient ID as stratum. **(B)** Volcano plot of KO gene families with respect to treatment time for all n = 40 patients. Points represent significantly enriched (blue) and depleted (orange) gene families (FDR < 0.2). **(C)** Gene set enrichment analysis of significantly enriched KOs from **(B)**. Gene sets with $p < 0.1$ are displayed. Pyrimidine metabolism-related pathways are bolded. **(D)** Fluoropyrimidine metabolism pathway with significantly enriched pyrimidine metabolism genes labeled in blue and 5-FU target thymidylate synthase (TS) labeled in green. **(E)** Microbes contributing to *preTA* in patient samples during treatment, with patients ordered by mean *preTA* abundance. **(F)** Sum of preTA+ *Escherichia*, *Anaerostipes*, *Eubacterium, Citrobacter* amplicon sequence variant (ASV) relative abundance by 16S sequencing. Solid line with shading represents LOESS interpolation mean±sem. **(G)** Comparison of *preTA*+ ASV abundance and *preTA* gene abundance. p-value: Spearman's rank correlation. **(H)** *preTA* levels are associated with 5-FU depletion in *ex vivo* communities incubated with 50 µg/mL 5-FU for 48 hours anaerobically. p-value: Spearman's rank correlation. **(I)** Microbes contributing to *preTA* in *ex vivo* communities. For **(G,H)**, solid lines represent a linear regression best fit with a shaded 95% confidence interval.

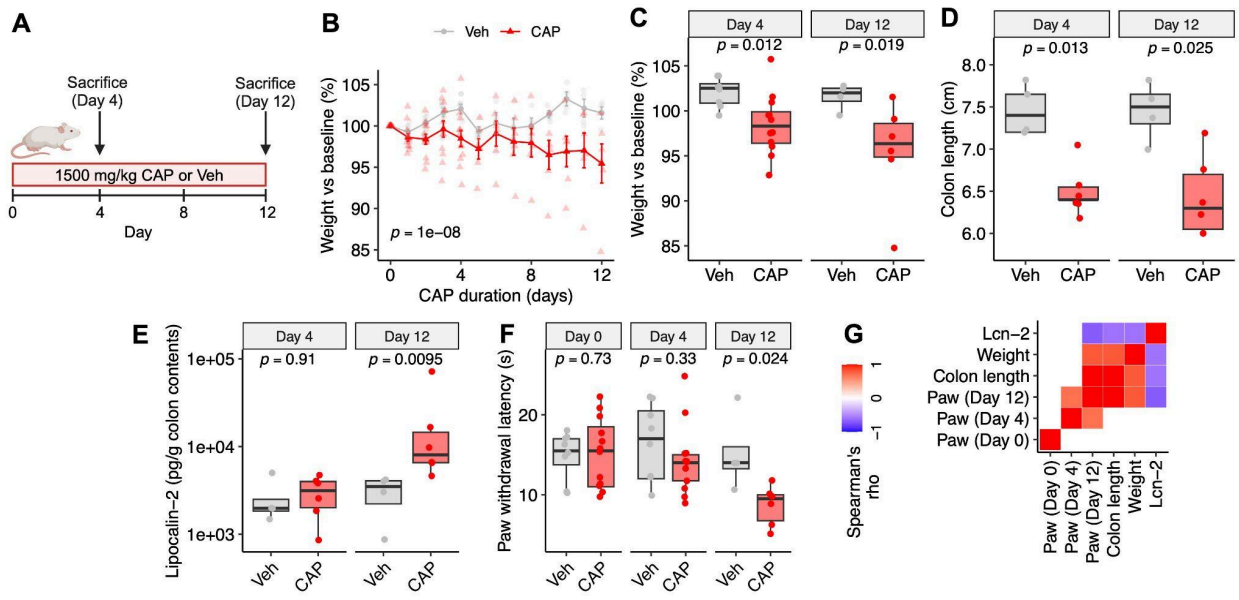

Figure 3: A mouse model of capecitabine (CAP) toxicity. (A) CAP toxicity mouse model. Mice were gavaged daily with 1500 mg/kg CAP (n = 12) or Vehicle (Veh, n = 8), with half the cohort sacrificed at Day 4. **(B)** Weight loss in CAP and Veh-treated mice. p-value: two-way ANOVA. **(C-F)** Toxicity endpoints at Day 4 and Day 12 of CAP treatment: mouse weight **(C)**, colon length **(D)**, lipocalin-2 in colon contents **(E)**, and hind paw withdrawal latency when placed on a 52°C hotplate **(F)**. p-values: Mann-Whitney U test. **(G)** Correlation of toxicity endpoints. All colored squares are significant (Spearman's correlation p-value < 0.05).

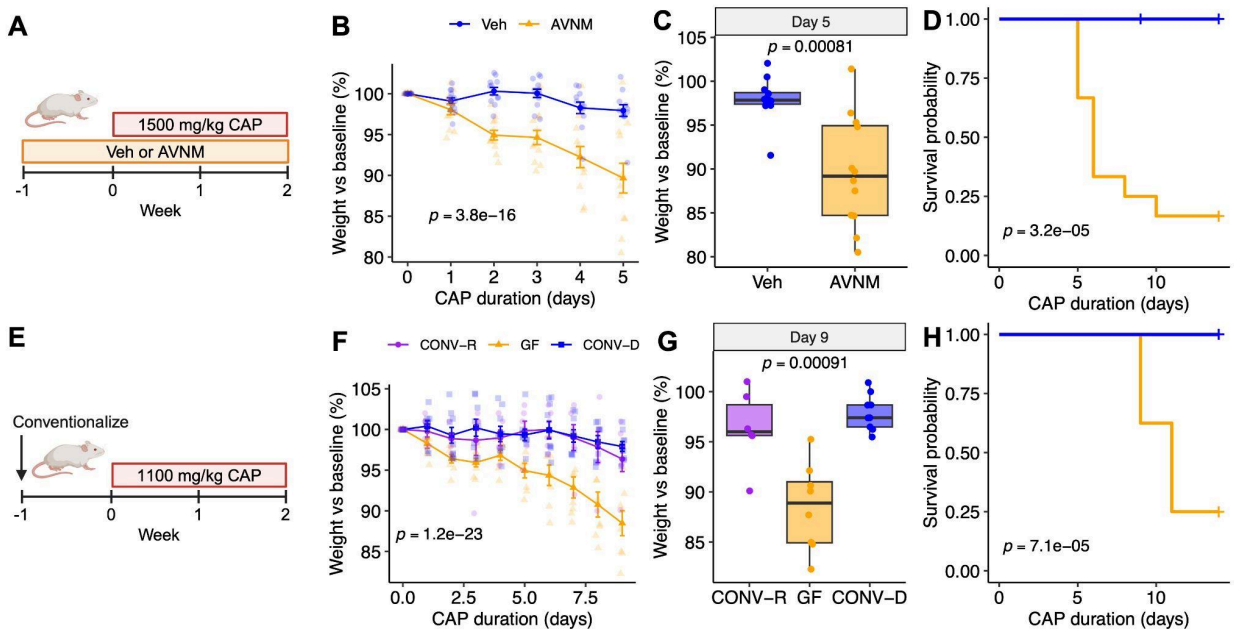

Figure 4: Microbiota depletion exacerbates capecitabine (CAP) toxicity in a mouse model. **(A)** AVNM antibiotic depletion CAP toxicity model. Mice were treated with AVNM (n = 12) or Vehicle (Veh, n = 12) for 1 week, then gavaged daily with 1500 mg/kg CAP. **(B)** CAP-induced weight loss in AVNM and Veh-treated mice. **(C)** Mouse weight on Day 5. p-value: Mann-Whitney U test. **(D)** CAP survival curve in AVNM and Veh treated mice. **(E)** CAP toxicity model in conventionally reared (CONV-R, n = 8), germ free (GF, n = 8), and conventionalized (CONV-D, n = 8) mice. **(F)** CAP-induced weight loss in CONV-R, GF, and CONV-D mice. **(G)** Mouse weight on Day 9. p-value: Kruskal-Wallis test. **(H)** CAP survival curve in CONV-R, GF, and CONV-D mice. **(B,F)** p-value: two-way ANOVA. **(D,H)** p-value: Mantel-Cox test.

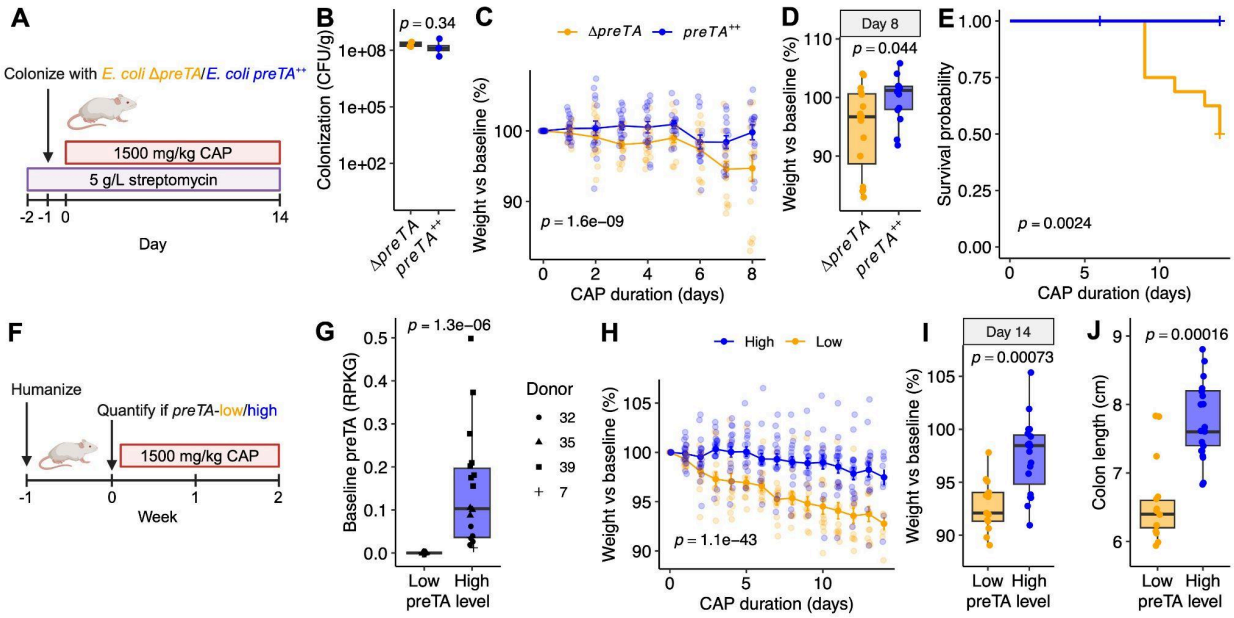

Figure 5: Microbial *preTA* rescues CAP toxicity. (A) *preTA* streptomycin (strep) colonization CAP toxicity model. Mice were treated with streptomycin for 1 day, gavaged with *E. coli* Δ*preTA* (n = 16) or *preTA*$^{++}$ (n = 16), then gavaged daily with 1500 mg/kg CAP. **(B)** *E. coli* colonization level**. (C)** CAP-induced weight loss in *preTA* strep colonization model. **(D)** Mouse weight on Day 8. **(E)** CAP survival curve in *preTA* strep colonization model. p-value: Mantel-Cox test. **(F)** *preTA* humanization CAP toxicity model. 32 mice were colonized with stool from GO patients for 1 week (n = 8/donor), then gavaged daily with 1500 mg/kg CAP. **(G)** Baseline *preTA* level in humanized mice and group assignments. **(H)** CAP-induced weight loss in *preTA* humanization CAP toxicity model. Endpoint mouse weight **(I)** and colon length **(J)**. **(B,D,G,I,J)** p-value: Mann-Whitney U Test. **(C,H)** p-value: two-way ANOVA.

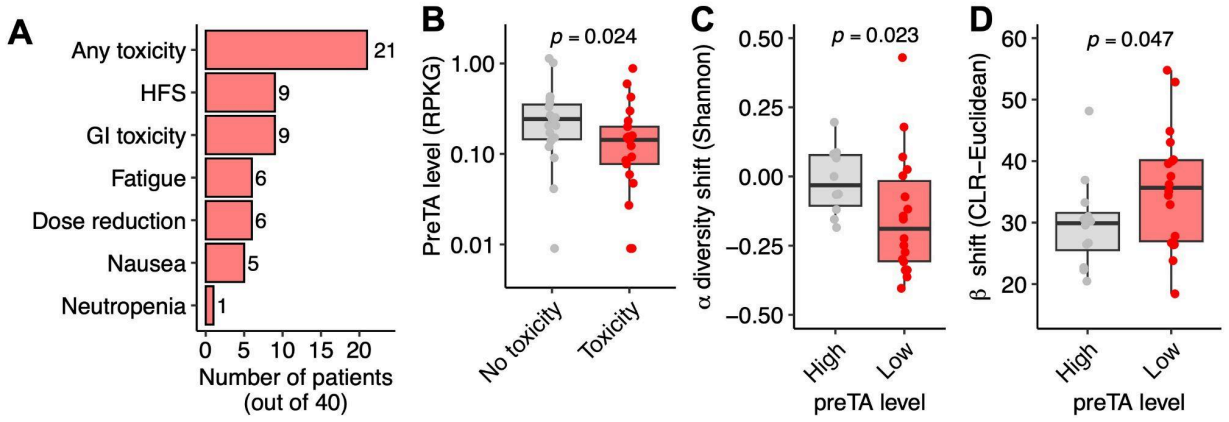

Figure 6: Microbial *preTA* is associated with oral fluoropyrimidine toxicity in patients. (A) Distribution of toxicities in GO patients. HFS: Hand-foot syndrome. **(B)** Patients experiencing toxicity have lower baseline stool microbial *preTA* levels (n = 40). p-value: one-sided Mann-Whitney U test. **(C)** *preTA* level (above/below mean) vs change in alpha diversity during Cycle 1 (C7D1-C1D1 Shannon index, n = 32). **(D)** *preTA* level (above/below mean) vs change in beta diversity during Cycle 1 (C7D1-C1D1 CLR-Euclidean distance, n = 32). **(C,D)** p-value: one-sided Wilcoxon signed-rank test.